Fractals, Vol. 11, No. 1 (2003) 39–52

World Scientific
www.worldscientific.com

THE EXQUISITE GEOMETRIC STRUCTURE OF A CENTRAL LIMIT THEOREM

CARLOS E. PUENTE
Hydrology and Institute of Theoretical Dynamics
University of California, Davis
Davis, CA 95616, USA
cepuente@ucdavis.edu

Received November 2, 2001; Accepted March 26, 2002

Abstract

Universal constructions of univariate and bivariate Gaussian distributions, as transformations of diffuse probability distributions via, respectively, plane- and space-filling fractal interpolating functions and the central limit theorems that they imply, are reviewed. It is illustrated that the construction of the bivariate Gaussian distribution yields exotic kaleidoscopic decompositions of the bell in terms of exquisite geometric structures which include non-trivial crystalline patterns having arbitrary n-fold symmetry, for any $n > 2$. It is shown that these results also hold when fractal interpolating functions are replaced by a more general class of attractors that are not functions.

Keywords: Central Limit Theorem; Fractal Interpolation; n-Fold Symmetric Patterns; Crystals.

1. INTRODUCTION

Recently, new universal constructions of the univariate and bivariate Gaussian distributions have been introduced.[1,2] Such representations rely on the usage of fractal interpolating functions[3] and measures supported by their graphs, in order to arrive at normal distributions as plane- or space-filling transformations of general diffuse measures.

The purpose of the present article is twofold. First, to provide a concise mathematical framework to the aforementioned formulations, including a suitable generalization of the ideas that results in Gaussian distributions from a class of more general attractors that are not functions. Second, to further illustrate the existence of a wide variety of exotic kaleidoscopic patterns that decompose the bivariate Gaussian distribution via the original formulation[4] and the subsequent extension of the ideas.

The organization of this paper is as follows. Section 2 reviews the required mathematical constructions that allow defining fractal interpolating functions and more general attractors over two or three dimensions and presents the implied Gaussian results obtained via these constructions over one and two dimensions. Section 3 illustrates the validity of the Gaussian results and presents, via examples, a host of the crystalline symmetric patterns that remarkably decompose bivariate Gaussian distributions. Finally, the article ends with its summary and with some final remarks.

2. MATHEMATICAL CONSTRUCTIONS AND PRACTICAL IMPLEMENTATION

The main mathematical results needed to establish the presence of sets of patterns that decompose the bivariate Gaussian distribution, for fractal interpolating functions and more general attractors, are given next. For completeness of presentation, the constructions start with fractal interpolating functions defined over two dimensions and yielding a univariate Gaussian distribution in the plane-filling case.

Theorem 2.1. Fractal Interpolating Functions in Two Dimensions (after Barnsley).[3] *Consider a set of $N+1$ non-aligned data points in the plane $\{(x_n, y_n); x_0 < \ldots < x_N, n = 0, 1, \ldots, N\}$ and N affine mappings having the special form*:

$$w_n \begin{pmatrix} x \\ y \end{pmatrix} = \begin{pmatrix} a_n & 0 \\ c_n & d_n \end{pmatrix} \begin{pmatrix} x \\ y \end{pmatrix} + \begin{pmatrix} e_n \\ f_n \end{pmatrix}, \quad n = 1, \ldots, N \quad (2.1)$$

with $0 \le |d_n| < 1$, and satisfying the conditions:

$$w_n \begin{pmatrix} x_0 \\ y_0 \end{pmatrix} = \begin{pmatrix} x_{n-1} \\ y_{n-1} \end{pmatrix}$$

$$w_n \begin{pmatrix} x_N \\ y_N \end{pmatrix} = \begin{pmatrix} x_n \\ y_n \end{pmatrix}, \quad n = 1, \ldots, N. \quad (2.2)$$

Then, G, the unique fixed-point of the affine mappings, i.e. $G = w_1(G) \cup \ldots \cup w_N(G)$, is the graph of a continuous function $f : [x_0, x_N] \to R$ that passes by the data points (i.e. $f(x_i) = y_i$, for $i = 0, 1, \ldots, N$), and has fractal dimension $D \in [1, 2)$ which is either the unique solution of $\sum |d_n| a_n^{D-1} = 1$ when $\sum |d_n| > 1$, or 1 otherwise. A function f so defined is termed a fractal interpolating function.

Remarks

(i) The proof of the existence and continuity of fractal interpolating functions is given in References 3 and 5.
(ii) Equations (2.1) and (2.2) result in N sets of four linear equations, from which the parameters a_n, c_n, e_n and f_n are computed in terms of the data points and the vertical scalings d_n.
(iii) The fractal dimension D tends to 2 when the magnitudes of all d_n's tend to 1. This implies, by considering every sign combination on the vertical scalings, the existence of 2^N routes toward obtaining plane-filling fractal interpolating functions.

Theorem 2.2. From a Diffuse Measure to the Univariate Gaussian Distribution via Plane-Filling Fractal Interpolating Functions (after Puente et al.)[1] *Consider a sequence of fractal interpolating functions f_i such that all of them interpolate the same set of non-aligned points in the plane $\{(x_n, y_n); x_0 < \ldots < x_N, n = 0, 1, \ldots, N\}$ and such that the graph G_i of such functions has fractal dimension D_i which tends to 2 as i tends to ∞. Let X be a diffuse probability measure over $I = [x_0, x_N]$, i.e. one that has a continuous cumulative distribution function and define the derived measures $Y_i(X) = X \circ f_i^{-1}$ and their standardized measures $Y_i^S(X)$, subtracting the mean and dividing by the standard deviation. Then, for any of the 2^N choices of sign combinations on the affine mappings scalings d_n's, $\lim_{i\to\infty} Y_i^S(X) = \mathcal{N}(0, 1)$ in distribution, where $\mathcal{N}(0, 1)$ is the standard Gaussian distribution with mean zero and variance one.*

Remarks

(i) The proof is accomplished via two steps.[1] First, the result is proven for a uniform parent measure $X = U$ over I by showing (by induction) that the moments of the standardized variables $Y_i^S(U)$ tend to those of the standard normal distribution, i.e. for all m, $\lim_{i\to\infty} E[Y_i^S(X)^{2m+1}] = 0$ and $\lim_{i\to\infty} E[Y_i^S(X)^{2m}] = 1 \cdot 3 \cdot \ldots \cdot (2m-1)$, where E is the expectation operator. Second, the theorem is extended to an arbitrary diffuse measure over I by demonstrating that the self-affinity of the limiting plane-filling function leads to Gaussian distributions within all successive N-ary restrictions of I as defined by iterations of the N affine mappings, distributions which when weighed by the corresponding parent measures on those subintervals give still a limiting Gaussian distribution.

(ii) Complete calculations for a single setup of sign combinations and for $N = 3$ are presented in Ref. 1.

(iii) The result is **universal** as the same limiting plane-filling function transforms a vast family of parent measures (with or without density functions) into the Gaussian.

(iv) As binomial multifractal measures and other singular measures encountered in the study of turbulence[6] may be used as natural parents[1] and as the bell is associated physically with the (slow) process of diffusion, the limiting plane-filling functions, by completely filtering the intermittency in turbulence into the harmonious bell, yield an unexpected relationship that transforms "violence" into "calmness." This intriguing result, although formally implied by Theorem 2.2, does not provide a concurrent physical interpretation, for calmness follows violence in nature.

(v) For the general case of a diffuse parent measure, it should be clarified that it is not a weighed sum of Gaussian random variables the one that turns out to be also Gaussian, but rather it is the sum of weighed Gaussian distributions the one that gives another Gaussian distribution.[1]

(vi) The construction implies a central limit theorem considering the following telescopic choice of random variables: $Y_i^T(X) = Y_i(X) - Y_{i-1}(X)$, $Y_0^T(X) = X$. But the result is not a trivial consequence of existing central limit theorems because the $Y_i^T(X)$'s, even though weakly dependent, are not identically distributed nor bounded (i.e. their variances tend to infinity).[1]

These two theorems are extended naturally to fractal interpolating functions over three dimensions as follows.

Theorem 2.3. Fractal Interpolating Functions in Three Dimensions (after Barnsley).[5] *Consider a set of $N + 1$ non-aligned data points $\{(x_n, y_n, z_n); x_0 < \ldots < x_N, n = 0, 1, \ldots, N\}$ and N affine mappings having the special form:*

$$w_n \begin{pmatrix} x \\ y \\ z \end{pmatrix} = \begin{pmatrix} a_n & 0 & 0 \\ c_n & d_n & h_n \\ k_n & l_n & m_n \end{pmatrix} \begin{pmatrix} x \\ y \\ z \end{pmatrix} + \begin{pmatrix} e_n \\ f_n \\ g_n \end{pmatrix}, \quad n = 1, \ldots, N \tag{2.3}$$

such that

$$A_n = \begin{pmatrix} d_n & h_n \\ l_n & m_n \end{pmatrix} = \begin{pmatrix} r_n^{(1)} \cos \theta_n^{(1)} & -r_n^{(2)} \sin \theta_n^{(2)} \\ r_n^{(1)} \sin \theta_n^{(1)} & r_n^{(2)} \cos \theta_n^{(2)} \end{pmatrix} \tag{2.4}$$

has L_2-norm less than 1 ($\|A_n\|_2 = \sqrt{\lambda_{\max}(A_n^T A_n)} < 1$) and subject to the conditions

$$w_n \begin{pmatrix} x_0 \\ y_0 \\ z_0 \end{pmatrix} = \begin{pmatrix} x_{n-1} \\ y_{n-1} \\ z_{n-1} \end{pmatrix}$$

$$w_n \begin{pmatrix} x_N \\ y_N \\ z_N \end{pmatrix} = \begin{pmatrix} x_n \\ y_n \\ z_n \end{pmatrix}, \quad n = 1, \ldots, N\,. \tag{2.5}$$

Then, G, the unique fixed-point of the affine mappings, i.e. $G = w_1(G) \cup \ldots \cup w_N(G)$, is the graph of a continuous function $f : [x_0, x_N] \to R^2$ that passes by the data points (i.e. $f(x_i) = (y_i, z_i)$, for $i = 0, 1, \ldots, N$), and has fractal dimension $D \in [1, 3)$ which depends on the coefficients a_n and the submatrix A_n. A function f so defined is termed a fractal interpolating function in three dimensions.

Remarks

(i) The proof of this theorem is completely analogous to the two-dimensional case and is given in Ref. 5.

(ii) Equations (2.3) and (2.5) result in N sets of six linear equations, from which the parameters a_n, c_n, k_n, e_n, f_n and g_n may be computed in terms of the data points and the scaling matrices A_n.

(iii) Increasingly space-filling fractal interpolating functions may be obtained as $\|A_n\|_2 \to 1$ for all n, which leads to the conditions $|r_n^{(j)}| \to 1$, $j = 1, 2$; $\theta_n^{(1)} \to \theta_n^{(2)} + k\pi$, for any integer k.[2]

This yields 4^N possible paths towards space-filling functions when considering all possible sign combinations on the parameters $r_n^{(j)}$.

Conjecture 2.1. From a Diffuse Measure to the Bivariate Gaussian Distribution via Space-Filling Fractal Interpolating Functions (after Puente and Klebanoff).[2] *Consider a sequence of three-dimensional fractal interpolating functions f_i such that all of them interpolate the same set of non-aligned points in three dimensions $\{(x_n, y_n, z_n); x_0 < \ldots < x_N, n = 0, 1, \ldots, N\}$ and such that the graph G_i of such functions has fractal dimension D_i which tends to 3 as i tends to ∞. Let X be a diffuse probability measure over $I = [x_0, x_N]$ and define the derived bivariate measures $(Y_i(X), Z_i(X)) = X \circ f_i^{-1}$ and their standardized bivariate measures $(Y_i^S(X), Z_i^S(X))$, subtracting their corresponding means and dividing by their standard deviations. Then, for any of the 4^N choices of sign combinations on the affine mappings parameters $r_n^{(j)}$'s, $\lim_{i\to\infty}(Y_i^S(X), Z_i^S(X)) = \mathcal{N}(0, 1, \rho)$, where $\mathcal{N}(0, 1, \rho)$ is a zero mean, variance one, bivariate Gaussian distribution, whose coefficient of correlation ρ depends on the data points, the choice of sign combinations on the $r_n^{(j)}$'s and the parent diffuse measure X.*

Remarks

(i) A general proof of the result following the steps of the one-dimensional case is not available at this time. This is because the joint moments of $(Y_i(U), Z_i(U))$ for a uniform measure U over I result in rather complicated formulas that preclude an elegant proof by induction.[2]

(ii) Available recursive formulas for the joint moments under the uniform case, obtained using the Maple V program, have allowed checking the validity of the result for joint order moments of orders up to 12.

(iii) For the uniform case when $N = 2$, four families of four sign combinations each on the $r_n^{(j)}$'s have been identified[2] that give different behavior in relation to the coefficient of correlation ρ. For the case when $\theta_n^{(1)} = \theta_n^{(2)} = \theta_n$, correlation zero happens almost everywhere in the plane $\theta_1 - \theta_2$. The four families give nonzero correlation at: (a) grid points multiples of π where ρ may jump to either 1 or -1, (b) horizontal lines where θ_2 is a multiple of π leading to continuously varying ρ's between -1 and 1 whose actual value depends on the data points, (c) vertical lines where θ_1 is a multiple of π and with a similar behavior to the previous case, and (d) inclined lines $\theta_1 = \theta_2 + k\pi$ where, once again, correlations vary continuously between -1 and 1 as a function of the data points.

(iv) Interesting cases have been identified[2] that allow explaining the coefficient of correlation of the bivariate Gaussian distribution in terms of the geometric similitude of the $x - y$ and $x - z$ projections of suitable space-filling fractal interpolating functions which are derived from a uniform distribution in x.

(v) As shall be illustrated later on, this conjecture has been verified computationally for a family of multinomial multifractal measures naturally induced in x.[1]

These results for fractal interpolating functions may be extended to encompass more general attractors as explained herein.

Theorem 2.4. General Attractors in Three Dimensions. *Consider a set of N affine mappings having the special form:*

$$w_n \begin{pmatrix} x \\ y \\ z \end{pmatrix} = \begin{pmatrix} a_n & 0 & 0 \\ c_n & d_n & h_n \\ k_n & l_n & m_n \end{pmatrix} \begin{pmatrix} x \\ y \\ z \end{pmatrix} + \begin{pmatrix} e_n \\ f_n \\ g_n \end{pmatrix}, \quad n = 1, \ldots, N \tag{2.6}$$

corresponding to left-right non-aligned end-data points $\{(x_l(n), y_l(n), z_l(n))\}$, $\{(x_r(n), y_r(n), z_r(n)\}$, i.e.

$$w_n \begin{pmatrix} x_l(1) \\ y_l(1) \\ z_l(1) \end{pmatrix} = \begin{pmatrix} x_l(n) \\ y_l(n) \\ z_l(n) \end{pmatrix}$$

$$w_n \begin{pmatrix} x_r(N) \\ y_r(N) \\ z_r(N) \end{pmatrix} = \begin{pmatrix} x_r(n) \\ y_r(n) \\ z_r(n) \end{pmatrix}, \quad n = 1, \ldots, N \tag{2.7}$$

with $x_l(1) = \min x_l(n)$, $x_r(N) = \max x_r(n)$,

$n = 1, \ldots, N$, and such that

$$A_n = \begin{pmatrix} d_n & h_n \\ l_n & m_n \end{pmatrix} = \begin{pmatrix} r_n^{(1)} \cos \theta_n^{(1)} & -r_n^{(2)} \sin \theta_n^{(2)} \\ r_n^{(1)} \sin \theta_n^{(1)} & r_n^{(2)} \cos \theta_n^{(2)} \end{pmatrix} \quad (2.8)$$

has L_2-norm less than 1. Then there is an attractor, G, the unique fixed-point of the affine mappings, i.e. $G = w_1(G) \cup \ldots \cup w_N(G)$, whose fractal dimension $D \in [0, 3)$ depends on the coefficients a_n and the submatrix A_n.

Remarks

(i) The proof of this theorem relies on the fact that all mappings involved are contractile.
(ii) Fractal interpolating points are obtained when the end-points yield a suitable set of interpolating points, i.e. $x_r(n) = x_l(n+1)$, $y_r(n) = y_l(n+1)$, $z_r(n) = z_l(n+1)$, $n = 1, \ldots, N-1$ and when the coordinates in x are ordered.
(iii) When the placement of end-points in x leaves holes within the domain interval $[x_l(1), x_r(N)]$, the resulting attractor is defined over a Cantor set. In those cases, the maximal attractor's dimension is the dimension of the Cantor set multiplied by three.
(iv) When the placement of end-points in x results in overlaps on the domains of affine mappings, the obtained fractal attractor is no longer a function. For these cases, the maximal attractor's dimension is three.
(v) As found for fractal interpolating functions, Eqs. (2.6) and (2.7) result in N sets of six linear equations, from which the parameters a_n, c_n, k_n, e_n, f_n and g_n may be computed in terms of the end-data points and the scaling matrices A_n.
(vi) As before, attractors that increasingly fill-up space may be obtained as $\|A_n\|_2 \to 1$ for all n, which leads to the conditions $|r_n^{(j)}| \to 1$, $j = 1, 2$; $\theta_n^{(1)} \to \theta_n^{(2)} + k\pi$, for any integer k. This yields, as before, 4^N possible paths towards maximal dimensions when considering all possible sign combinations on the parameters $r_n^{(j)}$.

Conjecture 2.2. From General Attractors of Maximal Dimension to the Bivariate Gaussian Distribution. *Consider a sequence of three-dimensional attractors G_i such that all are defined via suitable affine mappings given by the same set of non-aligned left-right end-points in three dimensions $\{(x_l(n), y_l(n), z_l(n))\}$, $\{(x_r(n), y_r(n), z_r(n)\}$, $x_l(1) = \min x_l(n)$, $x_r(N) = \max x_r(n)$, $n = 1, \ldots, N$, as in the previous theorem, and having increasing fractal dimensions D_i that tend to their maximal value (either three or such a value times the dimension of Cantor set over x) as i tends to ∞. Let M be a diffuse probability measure over G_i and define bivariate measures (Y_i, Z_i) as projections of M over the coordinates y and z and their standardized bivariate measures (Y_i^S, Z_i^S), subtracting their corresponding means and dividing by their standard deviations. Then, for any of the 4^N choices of sign combinations on the affine mappings parameters $r_n^{(j)}$'s, $\lim_{i\to\infty}(Y_i^S, Z_i^S) = \mathcal{N}(0, 1, \rho)$, where $\mathcal{N}(0, 1, \rho)$ is a zero mean, variance one, bivariate Gaussian distribution, whose coefficient of correlation ρ depends on the end-data points, the choice of sign combinations on the $r_n^{(j)}$'s and the measure M.*

Remarks

(i) This conjecture has been verified only computationally for a family of natural measures as generated over the attractor via the following implementation.

Theorem 2.5. An Ergodic Theorem for Computational Implementation (after Elton).[7] *Let G be the unique attractor associated with a set of contractile affine mappings w_n corresponding to left-right end-points $\{(x_l(n), y_l(n), z_l(n))\}$, $\{(x_r(n), y_r(n), z_r(n)\}$, $x_l(1) = \min x_l(n)$, $x_r(N) = \max x_r(n)$, $n = 1, \ldots, N$. Consider $\{(\bar{x}_m, \bar{y}_m, \bar{z}_m)\}$ a sequence of iterations as given by the corresponding mappings w_n, such that the maps are chosen independently according to a set of probabilities $p_1, \ldots, p_N$, starting at an arbitrary end-data point, say $(x_l(1), y_l(1), z_l(1))$, i.e.*

$$(\bar{x}_m, \bar{y}_m, \bar{z}_m) = w_{\sigma_m} \circ w_{\sigma_{m-1}} \circ \cdots \circ w_{\sigma_1}(x_l(1), y_l(1), z_l(1)) \qquad m = 1, 2, \ldots . \quad (2.9)$$

Then, there is a unique invariant measure $\tilde{M}$ induced by the sequence of iterations over the attractor G that defines unique projections over the x and $y-z$ coordinates that are respectively $X(\tilde{M})$ and

$(Y(\tilde{M}), Z(\tilde{M}))$. *Moreover, values gathered along an iteration path may be used with probability one, i.e. except for all code sequences* $\sigma_1, \sigma_2 \ldots$ *having probability zero, to calculate*

$$\lim_{m\to\infty} \frac{1}{m+1} \sum_{k=0}^{m} g(\bar{x}_k, \bar{y}_k, \bar{z}_k) = \int_{R^3} g(\vec{\mathbf{x}}) d\tilde{M}(\vec{\mathbf{x}}) \tag{2.10}$$

for all continuous functions $g : R^3 \to R$.

Remarks

(i) In case G defines a fractal interpolating function, the induced measures are as follows: in x, $X(\tilde{M})$ gives a multinomial multifractal measure over $[x_l(1), x_r(N)]$ with redistribution parameters p_n; in $y - z$, $(Y(\tilde{M}), Z(\tilde{M})) = X(\tilde{M}) \circ f^{-1}$ are defined as derived distributions. The existence of a unique measure $\tilde{M}$ over the graph of a fractal interpolating function is proven in Ref. 5.

(ii) In cases where the chosen end-points leave open some subintervals of $[x_l(1), x_r(N)]$, G becomes the product of the graph of a fractal interpolating function and a Cantor set.[1] For such cases, the measure $X(\tilde{M})$ is a multinomial multifractal over a Cantorian domain, with redistribution parameters p_n and scales as defined by the locations of the end-points in x. For this case, $(Y(\tilde{M}), Z(\tilde{M})) = X(\tilde{M}) \circ f^{-1}$ are also defined as derived distributions.

(iii) The theorem allows finding approximations of the measures $X(\tilde{M})$ and $(Y(\tilde{M}), Z(\tilde{M}))$ and their moments just by following a long branch of iterations. Examples obtained based on this implementation are given in the next section.

3. BIVARIATE GAUSSIAN DISTRIBUTIONS AND DECOMPOSITIONS

The examples that follow attempt to show that the aforementioned conjectures hold both for fractal interpolating functions and for the more general attractors. In the majority of graphs that follow, routine ran1[8] was used to define the corresponding single branch of affine mapping iterations, but an example obtained via the binary digits of π is also included.

Example 3.1. From a Binomial Multifractal to a Bivariate Gaussian via a Fractal Interpolating Function. Consider the generic set of interpolating points $\{(0, 0, 0), (1/2, 1, 1), (1, 0, 0)\}$, and $r_1^{(1)} = -r_2^{(1)} = r_1^{(2)} = -r_2^{(2)} = 0.9995$, $\theta_1 = \theta_2 = \pi/5$, and a path of iterations that extends for 15 million nodes starting at the mid-point and going left 70% and right 30% of the time, computed using the routine ran1 with seed -123. Figure 1 shows the resulting projections in $x-y$ and $x-z$ of the graph of

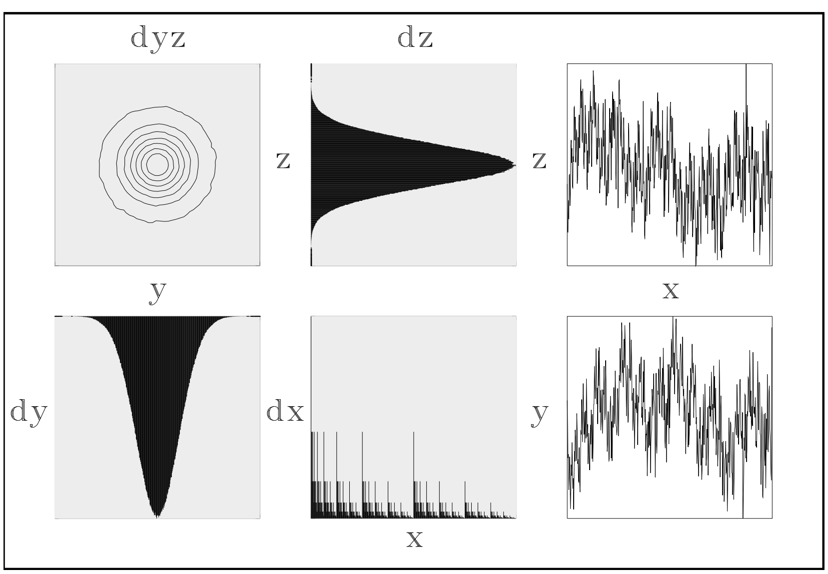

Fig. 1 A bivariate Gaussian distribution from a fractal interpolating function and a binomial multifractal measure. *Range on bivariate measure*: -94, 96.

the fractal interpolating function and a close approximation to a bivariate Gaussian distribution with no correlation, as indicated by the marginal densities dy and dz and the circular contours on the joint measure dyz, based on a binomial multifractal measure dx.

Remarks

(i) The shown projections of the fractal interpolating function are only approximate renderings of the true objects. They were found averaging all points (of the 15 million) that fall on each of 512 equally sized subintervals in x. For aesthetic purposes, these averaged graphs were stretched vertically on the plot so that they occupy all the available space.

(ii) Other sign combinations on the scaling parameters and arbitrary angles θ_1 and θ_2 also lead to similar graphs, possibly with nonzero correlation.

Example 3.2. A Circular Bell via a General Attractor. Consider the set of left-right end-points $\{(0, 0, 0), (0.7, 2, 1)\}$, $\{(1/2, 1, 1), (1, 0, 0)\}$, $r_1^{(1)} = -r_2^{(1)} = r_1^{(2)} = -r_2^{(2)} = 0.9995$, $\theta_1 = \theta_2 = \pi/5$, and a path of iterations that extends for 15 million nodes starting at $(1/2, 1, 1)$ and using the two affine mappings 70 and 30% of the time, via the routine ran1 with seed -123. Figure 2 shows the analogous of Fig. 1, found projecting the unique measure on the general attractor over the three coordinates. As may be seen, a close approximation to a bivariate Gaussian distribution is also found.

Remarks

(i) The obtained measure in x, dx, is no longer a simple binomial multifractal as the end-points that define the contractions on the affine mappings overlap.

(ii) The shown projections of the attractor over xy and xz are smoothed renderings of attractor which indeed is not a function. As in the previous example, they were found averaging all points (of the 15 million) that fall on each of 512 equally sized subintervals in x. For aesthetic purposes, these graphs were stretched vertically on the plot so that they occupy all the available space.

(iii) As found with fractal interpolating functions, other sign combinations on the scaling parameters and arbitrary angles θ_1 and θ_2 also lead to similar graphs, possibly with nonzero correlation.

Example 3.3. Sequential Patterns Inside the Bell from Fractal Interpolating Functions. Consider the generic set of interpolating points $\{(0, 0, 0), (1/2, 1, 1), (1, 0, 0)\}$, $r_1^{(1)} = -r_2^{(1)} = r_1^{(2)} = -r_2^{(2)} = 0.9999$, $\theta_1 = \theta_2 = \pi/5$, and the same seed of -123

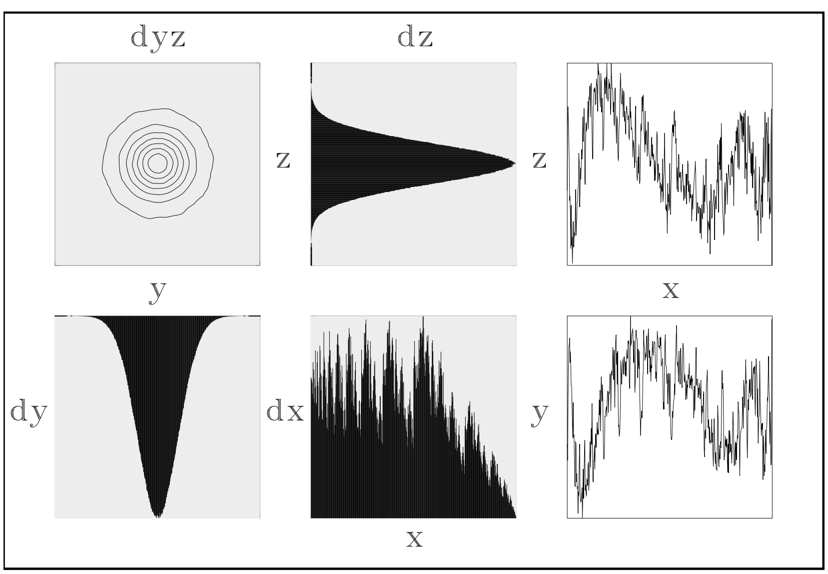

Fig. 2 A bivariate Gaussian distribution from a general attractor. *Range on bivariate measure*: -146, 147.

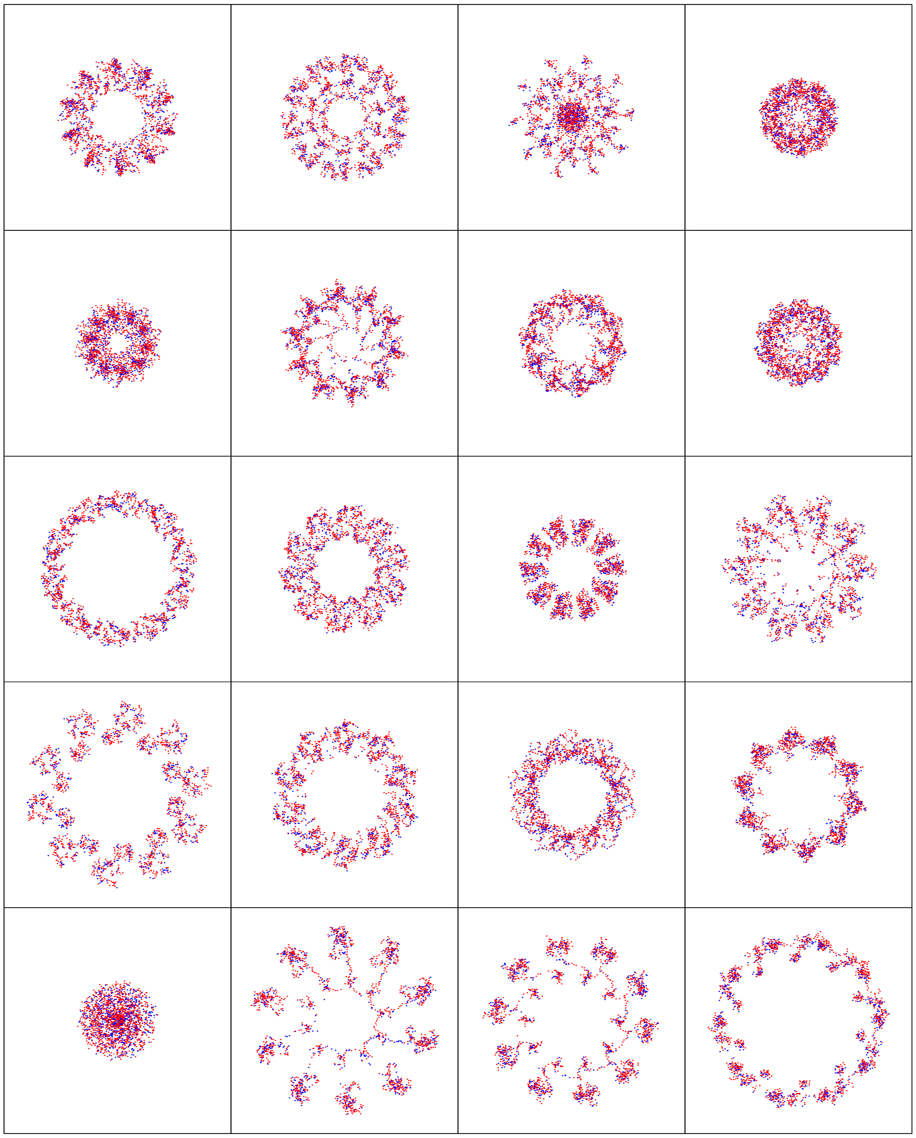

Fig. 3 Sequential patterns inside the circular bell from a fractal interpolating function. *Range on squares*: −104, 104.

for ran1 as used in the previous examples. But instead of 15 million iterations, study the behavior of the first $40,000$ dots over the $y-z$ plane using w_1 70% and w_2 30% of the time. Figure 3 shows the corresponding 20 frames of 2000 dots each, colored according to the used affine mapping, from left to right and from bottom to top. As seen, behavior is not just circular but rather leads to exotic patterns with ten-fold symmetry, i.e. 2π over $\pi/5$.

Remarks

(i) Continuing the generation every 2000 dots gives additional pages whose crystal-like kaleidoscopic behavior does not repeat in any trivial manner. These patterns provide an unexpected decomposition of the circular bivariate Gaussian distribution.

(ii) Usage of other seeds to drive routine ran1 or use of the digits of irrational numbers, e.g. π (modulus 2), gives yet, as shall be shown later, other exotic patterns that decompose the circular bell.[4] This also happens when points in x are taken not equally spaced.

(iii) By varying the angles θ_1 and θ_2, a great variety of decompositions having arbitrary symmetries may be generated. For integer-valued angles in degrees, the actual number of tips on the figures are basically $nt = 2\pi/\theta$, where θ is the maximum common divisor between θ_1

and θ_2. But, depending on the sign combination of the scaling parameters the tips may be twice or half nt.

(iv) There are cases, for nt large and for suitable sign combinations on the scalings, when circular disks and rings "dance in and out" making up a circular bell. This behavior is not common to all possible scenarios as there are sign combinations within the same overall setup which lead to crystal-like patterns.

(v) Not all patterns inside the bell are found to have the same degree of geometrical definition and symmetry. The actual "fuzziness" decreases as the magnitude of the scaling parameters tends towards 1, but it also depends, in a nontrivial manner, on: (i) the actual path of iterations, (ii) the angles used, and (iii) the sign combinations of the scalings.

(vi) The sign combinations cases on the scaling parameters that generate Gaussians with arbitrary correlations, as mentioned earlier,[2] serve to define exotic decompositions of elliptical bells. Typically, these are not just "elliptical" renditions similar to those shown in Fig. 3, but rather such sets are made of stretched broken patterns aligned with the major axes of the limiting ellipse.

(vii) Yet other decompositions are found having more than three interpolating points and choosing the path of iterations such that

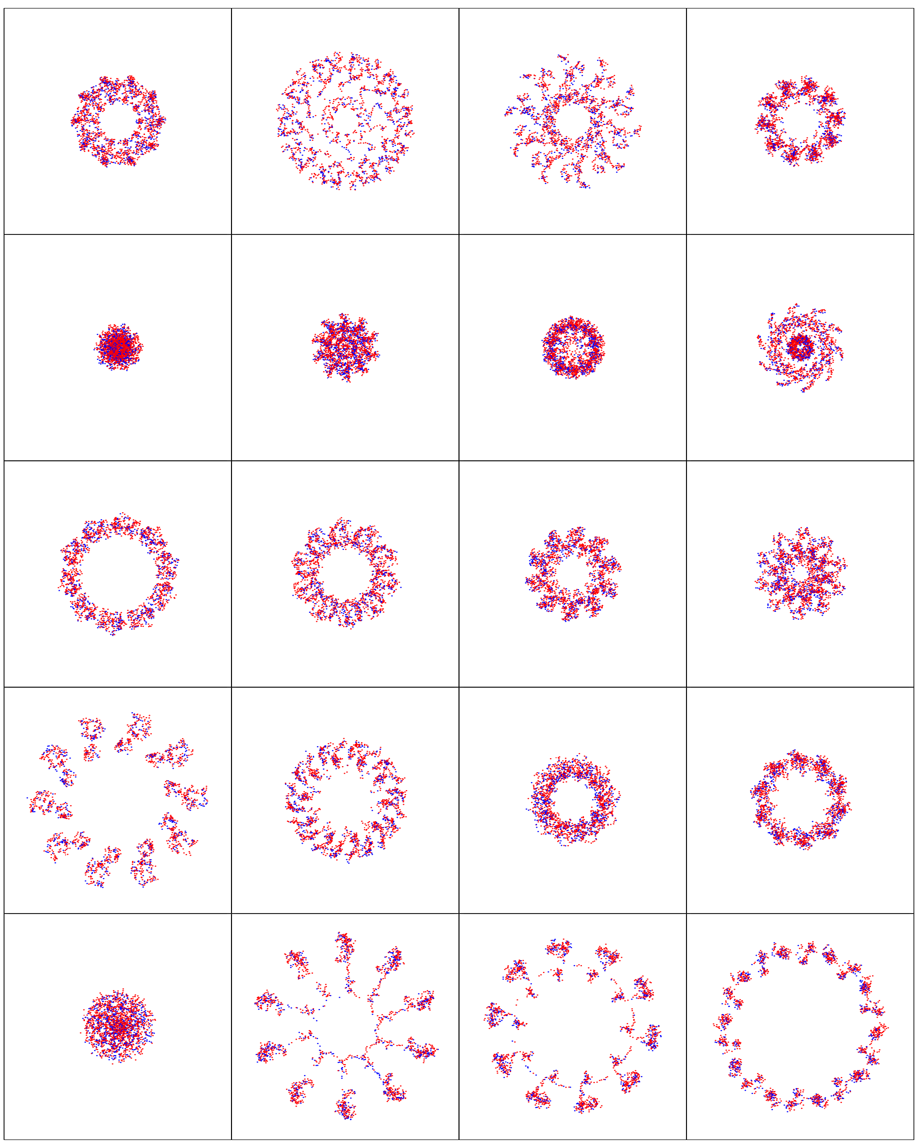

Fig. 4 Sequential patterns inside the circular bell from a general attractor. *Range on squares*: −173, 173.

arbitrary multinomial multifractals (with arbitrary length scales) are generated over the domain of the unique fractal interpolating function in x.

(viii) Some interesting patterns illustrating some of these remarks are presented later on.

Example 3.4. Sequential Patterns Inside the Bell from General Attractors. Consider the previously chosen end-points $\{(0, 0, 0), (0.7, 2, 1)\}$, $\{(1/2, 1, 1), (1, 0, 0)\}$, $r_1^{(1)} = -r_2^{(1)} = r_1^{(2)} = -r_2^{(2)} = 0.9999$, $\theta_1 = \theta_2 = \pi/5$, and the same seed of -123 for ran1 as used in the previous examples. But instead of 15 million iterations, study the behavior of the first $40,000$ dots over the $y - z$ plane using w_1 70% and w_2 30% of the time. Figure 4 shows the analogous of Fig. 3 corresponding to 20 frames of 2000 dots each, colored according to the used affine mapping, from left to right and from bottom to top. As seen, behavior for the general attractor also leads to exotic patterns with ten-fold symmetry, i.e. 2π over $\pi/5$.

Remarks

(i) Qualitatively, all remarks made about kaleidoscopic patterns generated by fractal interpolating also hold for the more general attractors (Cantorian or otherwise). As may be hinted, the nature of the decompositions depends on the angles θ_1 and θ_2, the specific sign combinations on the scaling parameters $r_n^{(j)}$, and the actual placings of the affine mappings' end-points.

As the decompositions inside the bell are rather beautiful, some examples based on fractal interpolating functions are given next. For clarity of presentation, all these sets are defined via the generic set of interpolating points $\{(0, 0, 0), (1/2, 1, 1), (1, 0, 0)\}$.

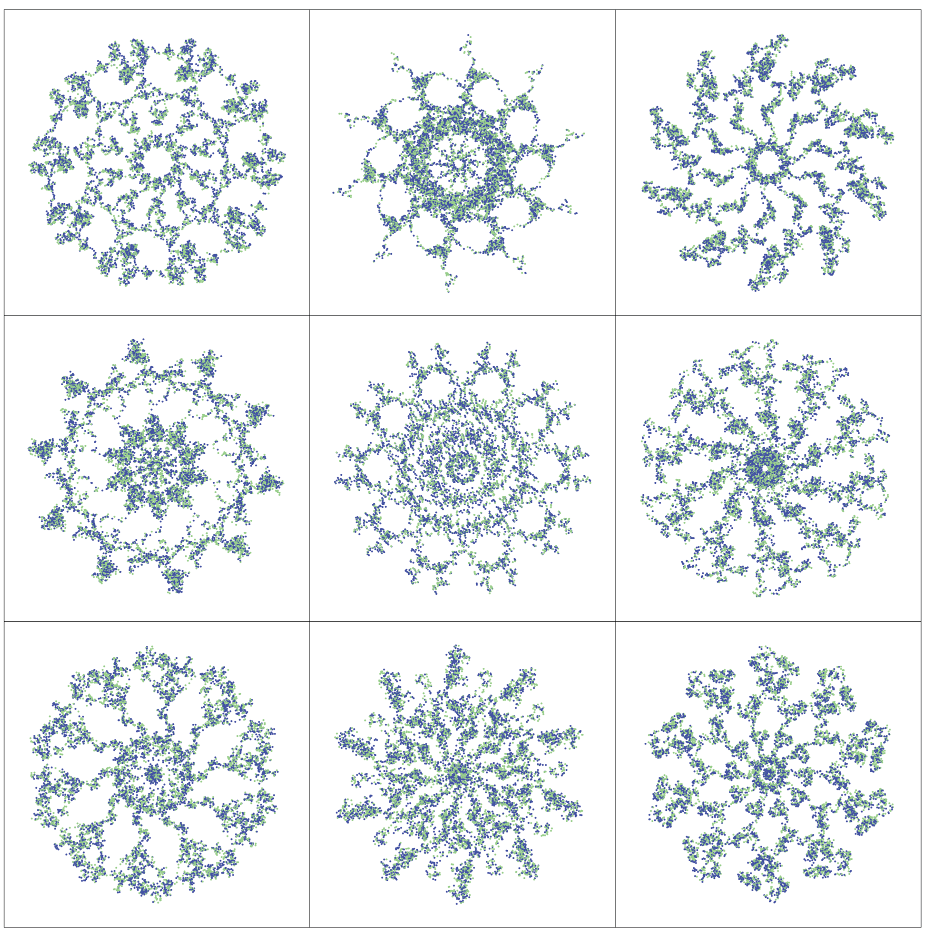

Fig. 5 Selected patterns with ten-fold symmetry inside the circular bell (see Table 1).

Example 3.5. Selected Patterns of Ten-Fold Symmetry Inside the Bell. Figure 5 shows nine patterns of 10,000 dots each, all sharing $\theta_1 = \theta_2 = \pi/5$ and scaling magnitudes equal to 0.99999, but found following alternative paths of iterations which use w_1 and w_2 each 50% of the time. These patterns, with key characteristics summarized in Table 1, are not sequential nor equal in size, but have been plotted stretched so that they occupy all available space. As may be seen, some patterns exhibit radial symmetry, while others, as in Figs. 3 and 4, appear to rotate.

Table 1 Parameters of Fig. 5. From left to right and bottom to top.

$r_1^{(1)}$	$r_1^{(2)}$	$r_2^{(1)}$	$r_2^{(2)}$	Seed	Initial Point	Squares' Ranges
+	+	+	+	−700	1	−70, 72
+	+	+	+	−23	1	−64, 66
−	+	−	+	−23	1	−143, 142
+	+	+	+	−80	1	−75, 75
+	−	+	+	−276	1	−299, 298
+	+	+	+	−111	1	−72, 74
+	−	+	−	−60	10001	−143, 143
+	+	+	+	−864	30001	−74, 77
−	+	−	+	−666	10001	−169, 170

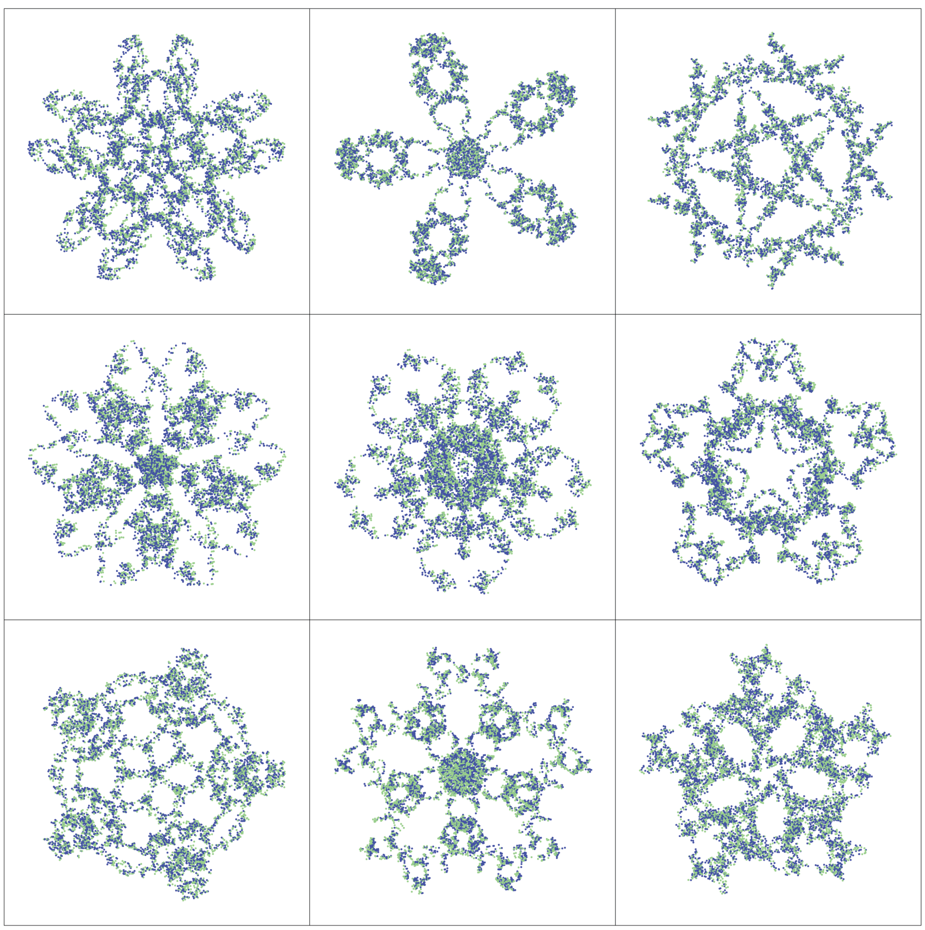

Fig. 6 Selected patterns with five-fold symmetry inside the circular bell (see Table 2).

Example 3.6. Selected Patterns of Five-Fold Symmetry Inside the Bell. Figure 6 parallels the previous example but has exotic figures with five tips, with key characteristic given in Table 2.

Example 3.7. Selected Patterns of Arbitrary Symmetry Inside the Bell. Figure 7 provides patterns of $10,000$ dots each that are found varying the angles θ_1 and θ_2 while maintaining the scalings

Table 2 Parameters of Fig. 6. From left to right and bottom to top.

$r_1^{(1)}$	$r_1^{(2)}$	$r_2^{(1)}$	$r_2^{(2)}$	Seed	Initial Point	Squares' Ranges
$-$	$-$	$+$	$-$	-60	1	$-84, 86$
$+$	$-$	$-$	$-$	-555	20001	$-87, 88$
$-$	$-$	$-$	$-$	-555	30001	$-55, 57$
$-$	$+$	$-$	$-$	-13	10001	$-66, 67$
$-$	$+$	$-$	$-$	-80	1	$-70, 70$
$-$	$+$	$-$	$-$	-80	10001	$-87, 88$
$-$	$+$	$-$	$-$	-8	1	$-85, 86$
$-$	$-$	$-$	$+$	-60	1	$-116, 112$
$-$	$-$	$-$	$+$	-700	10001	$-103, 102$

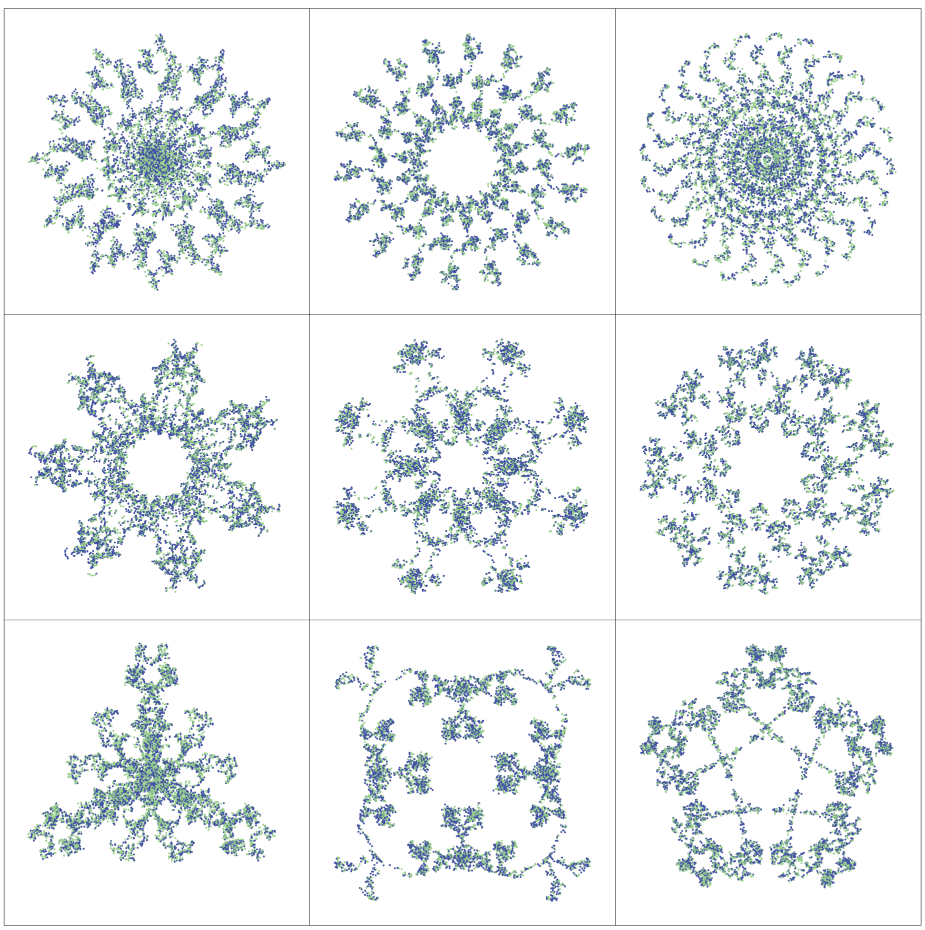

Fig. 7 Selected patterns with three-, four-, five-, seven-, eight-, nine-, 12-, 18-, and 24-fold symmetry inside the circular bell (see Table 3).

Table 3 Parameters of Fig. 7. From left to right and bottom to top.

$r_1^{(1)}$	$r_1^{(2)}$	$r_2^{(1)}$	$r_2^{(2)}$	θ_1	θ_2	Seed	Initial Point	Squares' Ranges
$-$	$+$	$+$	$+$	$2\pi/3$	$4\pi/3$	-60	30001	$-56, 61$
$-$	$-$	$-$	$+$	$\pi/2$	π	-80	30001	$-130, 131$
$+$	$-$	$+$	$+$	$2\pi/5$	$4\pi/5$	-80	20001	$-173, 177$
$+$	$+$	$+$	$-$	$2\pi/7$	$4\pi/7$	-60	20001	$-364, 359$
$+$	$-$	$+$	$+$	$\pi/4$	$\pi/3$	-80	30001	$-80, 81$
$+$	$+$	$+$	$-$	$2\pi/9$	$4\pi/9$	-80	10001	$-647, 654$
$+$	$-$	$+$	$-$	$\pi/6$	$\pi/3$	-80	1	$-138, 139$
$-$	$-$	$-$	$-$	$\pi/9$	$2\pi/9$	-60	10001	$-131, 133$
$+$	$+$	$+$	$+$	$\pi/12$	$\pi/6$	-60	1	$-123, 123$

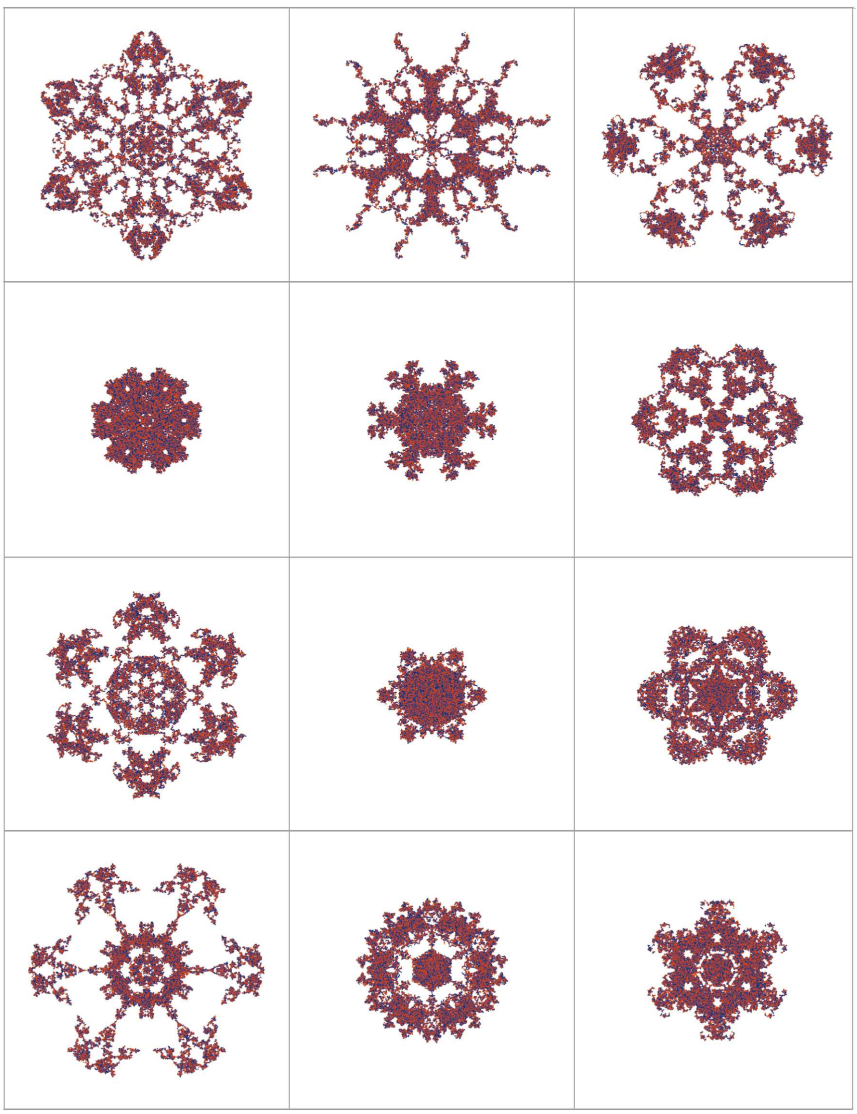

Fig. 8 Selected patterns with six-fold symmetry inside the circular bell via the binary digits of π. *Range on squares*: -867, 866.

magnitude at 0.99999. The key characteristics of these patterns are given in Table 3.

Example 3.8. Selected Patterns of Six-Fold Symmetry Inside the Bell Encoded by the Binary Digits of π. Consider $r_1^{(1)} = r_2^{(1)} = r_1^{(2)} = -r_2^{(2)} = 0.9999999999$, $\theta_1 = \theta_2 = \pi/3$, and the binary expansion of π in groups of 100,000 digits to select alternative paths of iterations. Figure 8 shows the corresponding 12 frames of $100,000$ dots each, colored according to the used affine mapping, from left to right and from bottom to top, that result if the iterations process is started for all frames from the mid-point (1/2, 1, 1). The largest pattern dictates the scale of all frames.

4. SUMMARY AND FINAL REMARKS

As illustrated in this work, there are exquisite crystalline symmetric patterns that decompose the bell in nontrivial kaleidoscopic manners. These sets are concealed inside the bell and are made explicit via suitable affine mapping iterations that define fractal interpolating functions or other general attractors that are not functions.

As the same unique fractal interpolating function (or general attractor) is obtained irrespective of the path of sequential iterations made, patterns obtained via alternative seeds may be added (after proper standardization) to yield a bivariate bell as the final outcome of a gigantic jigsaw puzzle. In the same spirit, patterns corresponding to different symmetries may be added together (after proper standardization) to yield even larger puzzles that decompose the bell in nontrivial ways.

Interestingly, some of the kaleidoscopic patterns inside the bell resemble the geometric structure of relevant natural objects that include: flowers, spiral galaxies, diatoms, marine microorganisms, snow crystals, viruses, proteins, and projections of DNA in two-dimensions.[9,10] Examples of these patterns shall be presented in Ref. 11.

Although similar symmetric patterns to those shown here may be obtained via nonlinear approaches that do not necessarily lead to the bivariate bell,[12] it is not known at this stage if usage of affine mappings fully characterize all the symmetric patterns concealed inside the bell. Also whether the ideas may be extended so that they define other patterns inside other suitable limiting distributions (e.g. Levy measures) is an open question.

ACKNOWLEDGMENTS

The author dedicates this work to Marta, Cristina, and Mariana. The financial support of Pacific Telesis is warmly appreciated. Discussions with Nelson Obregón, Oscar Robayo, Marta G. Puente, John Wagner, Akin Orhun and Bellie Sivakumar are gratefully acknowledged.

REFERENCES

1. C. E. Puente, M. M. López, J. E. Pinzón and J. M. Angulo, "The Gaussian Distribution Revisited," *Adv. Appl. Prob.* **28**(2), 500–524 (1996).
2. C. E. Puente and A. Klebanoff, "Gaussians Everywhere," *Fractals* **2**(1), 65–79 (1994).
3. M. F. Barnsley, "Fractal Functions and Interpolation," *Constr. Approx.* **2**, 303–329 (1986).
4. C. E. Puente, "The Remarkable Kaleidoscopic Decompositions of the Bivariate Gaussian Distribution," *Fractals* **5**(1), 47–61 (1997).
5. M. F. Barnsley, *Fractals Everywhere* (Academic Press, New York, 1988).
6. K. R. Sreenivasan, "Fractals and Multifractals in Fluid Turbulence," *Ann. Rev. Fluid Mech.* **23**, 539–600 (1991).
7. J. Elton, "An Ergodic Theorem for Iterated Maps," *J. Erg. The. Dynam. Syst.* **7**, 481–488 (1987).
8. W. H. Press, S. A. Teukolsky, W. T. Vetterling and B. P. Flannery, *Numerical Recipes. The Art of Scientific Computing* (Cambridge University Press, 1989).
9. C. E. Puente, N. Obregón, O. Robayo, M. G. Puente and D. Simsek, "Projections Off Fractal Functions: A New Vision of Nature's Complexity," *Fractals* **7**(4), 387–401 (1999).
10. C. E. Puente, "DNA, Pi and the Bell," *Complexity* **6**(2), 16–22 (2000).
11. C. E. Puente, *Treasures Inside the Bell. Hidden Order in Chance* (World Scientific, 2002), in press.
12. G. M. Zaslavsky, *Physics of Chaos in Hamiltonian Systems* (Imperial College Press, London, 1998).